

www.acsnano.org

Spectrum of Exfoliable 1D van der Waals Molecular Wires and Their Electronic **Properties**

Yanbing Zhu, Daniel A. Rehn, Evan R. Antoniuk, Gowoon Cheon, Rodrigo Freitas, Aditi Krishnapriyan, and Evan J. Reed*



Cite This: ACS Nano 2021, 15, 9851-9859



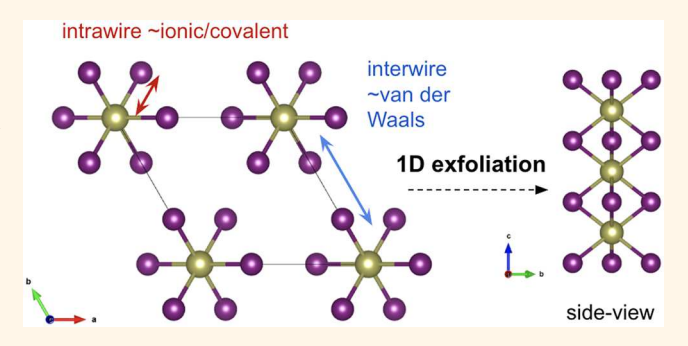
ACCESS I

Metrics & More

Article Recommendations

Supporting Information

ABSTRACT: Two-dimensional (2D) materials derived from van der Waals (vdW)-bonded layered crystals have been the subject of considerable research focus, but their one-dimensional (1D) analogues have received less attention. These bulk crystals consist of covalently bonded multiatom atomic chains with weak van der Waals bonds between adjacent chains. Using density-functional-theory-based methods, we find the binding energies of several 1D families of materials to be within typical exfoliation ranges possible for 2D materials. In addition, we compute the electronic properties of a variety of insulating, semiconducting, and metallic individual wires and find differences that could enable the identification of and distinction



between 1D, 2D, and 3D forms during mechanical exfoliation onto a substrate. We find 1D wires from chemical families of the forms PdBr2, SbSeI, and GePdS3 are likely to be distinguishable from bulk materials via photoluminescence. Like 2D vdW materials, we find some of these 1D vdW materials have the potential to retain their bulk properties down to nearly atomic film thicknesses, including the structural families of HfI₃ and PNF₂, a useful property for some applications including electronic interconnects. We also study naturally occurring bulk crystalline heterostructures of 1D wires and identify two families that are likely to be exfoliable and identifiable as individual 1D wire subcomponents.

KEYWORDS: van der Waals materials, one-dimensional wires, layered heterostructures, photoluminescence, exfoliation

ulk crystals consisting of weakly bonded one-dimensional wires have been proposed to play a role alongside 2D materials as an increasing number of van der Waals (vdW)-based devices are developed for electronic interconnect, transistor, and memory applications. 1-5 Data mining of crystal structure databases suggests there are hundreds of such crystals synthesized and characterized over recent decades. This number is on par with the approximately 1800 reported bulk crystals that are likely to be exfoliable into 2D layers. The van der Waals wires studied are quasi-one-dimensional, owing to their finite radii that are typically a nanometer or lower. Such bulk structures can grow in wire bundles with diameters that increase in discrete increments, which are analogous to 2D van der Waals materials characterized by layer number.

The presumed lack of dangling surface bonds due to weak van der Waals interactions between adjacent wires can allow wires to retain close-to-bulk characteristics at nanometer-scale radial dimensions, a useful property for electronic applications. Existing electronic interconnect materials such as copper (Cu) exhibit an inverse relationship between resistance and wire size at the nanometer scale due to increased surface roughness and grain boundary scattering,⁸⁻¹¹ placing a limit on the scaling down of the size of Cu wires. This effect is also reported in bismuth (Bi)¹² and gold (Au)¹³ nanowires. While carbon nanotubes and wider nanoribbon structures have been proposed as alternatives, they exhibit electronic properties that change significantly based on chirality, edge terminations, and size including Wigner crystal, Kondo physics, and Luttinger liquid behavior. $^{14-17}$

One-dimensional materials beyond nanotubes and bulkmaterial-based nanowires include organic and polymer chains,

Received: January 27, 2021 Accepted: May 19, 2021 Published: May 28, 2021





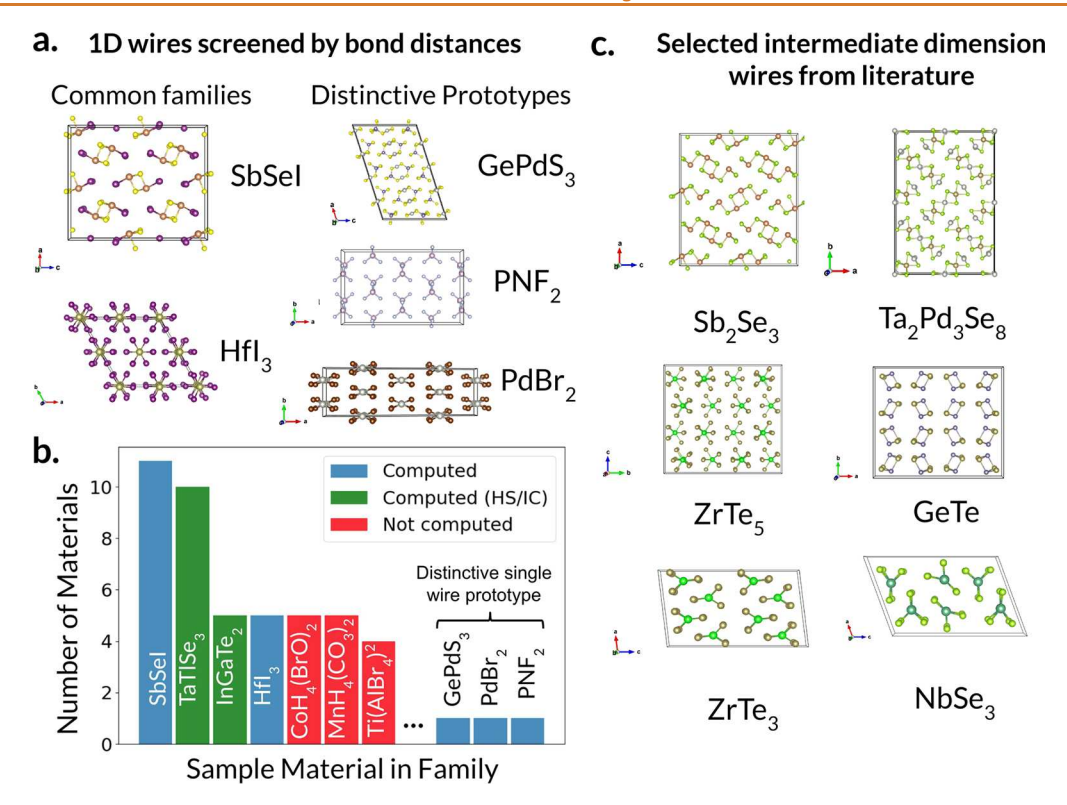


Figure 1. (a) Selected wire structure from previous screening,⁶ for which electronic structure calculations are performed. Wires are shown at the top in a 2 × 2 supercell geometry taken in the directions normal to the wire to allow for sufficient vacuum when the individual wire is extracted. (b) Distribution of the common families of 1D wires. Blue indicates wire structures studied in this work. Green indicates studied heterostructures or intercalated materials where the compound consists of wires of different compositions as detailed in Figure 4. Red indicates common families not studied in detail here. (c) Additional intermediate-dimension wire structures that did not appear in the 1D screening but have been previously studied experimentally. These materials exhibit dimensionality intermediate between 1D wires, 2D layers, and bulk 3D materials. Analogous DFT calculations are performed for these structures as a benchmark.

the charge transfer salt TTF-TCNQ₁¹⁸ $K_2Pt(CN)_4Br_{0.3}$. 3.2 H_2O containing a 1D chain of Pt atoms¹⁹ studied in the context of high-temperature superconductivity, and the linear chain polymers $(SN)_x$ and $(CH)_x$, where the latter is polyacetylene and theoretically studied in the Su–Schrieffer–Heeger model.²⁰

The small diameter and 1D nature of van der Waals wires allows additional control over electronic properties through the application of external stimuli, such as strain or electrostatic gating. Such wires may support potential applications in not only electronics but also photonics and optoelectronics with the downscaling of component sizes. 1D materials such as TaSe₃ have been demonstrated to exhibit high breakdown current densities an order of magnitude larger than Cu.²¹

Limited work exists on the properties and exfoliation potential of individual wire chains or layers of chains within the framework of van der Waals materials. *Ab initio* calculations have been performed on single linear chains of individual atoms such as Fe, Ge, Au, and Te^{22–25} as well as different geometries of common nanowire materials SiC, GaN, BN, ZnO, ZnS, and CdS.²⁶ The materials studied in this work are more complex, extending beyond monatomic or common semiconducting materials, and are known to be stable in the bulk form composed of intrinsically 1D chains.

Analogous calculations exist for specific classes of 1D materials such as SbSeI, SbSI, and SbSBr, ²⁷ and there exists a report of successfully exfoliated 1D van der Waals materials Ta₂Pd₃Se₈. ²⁸ Materials in the transition metal trichalcogenide family MX₃ have been exfoliated using shear forces using an

atomic force microscope (AFM) tip, ²⁹ in addition to a recent ground-up synthesis of multiple wire structures using chemical vapor deposition (CVD). Further experimental efforts include single-atom chains of Te extracted by dragging a single-crystal bulk sample across a substrate²⁵ and isolation of Sb₂Se₃ nanoribbons obtained using liquid water intercalation and separation by the expansion force from freezing.³⁰ While mechanical exfoliation is so far reported to be less effective for 1D materials compared to 2D materials,³⁰ previous work suggests other extraction methods are possible. The relationship between the band structure change upon exfoliation, binding energies, and different wire geometries investigated is useful information that has received relatively little attention.

Among the key challenges associated with isolating and studying such small diameter 1D structures is identifying them on a substrate. While atomically thin 2D materials can be identified with optical microscopy when on a suitable substrate, identification of 1D wires using this approach is likely not feasible. Here, we address this challenge by computing electronic signatures of 1D wires that could potentially be exploited for differentiation between 1D wires, 2D films, and bulk *via* photoluminescence.

We note the commonly employed terminology of nanowires, nanotubes, and nanoribbons does not necessarily reflect size. The wires in this study have smaller radial dimensions than typical structures referred to as nanowires, ribbons, or tubes, but this is not always true. The smallest carbon "nanotube" grown to date is 3 Å in diameter grown inside a multiwalled carbon nanotube, ³¹ and the smallest free-standing carbon

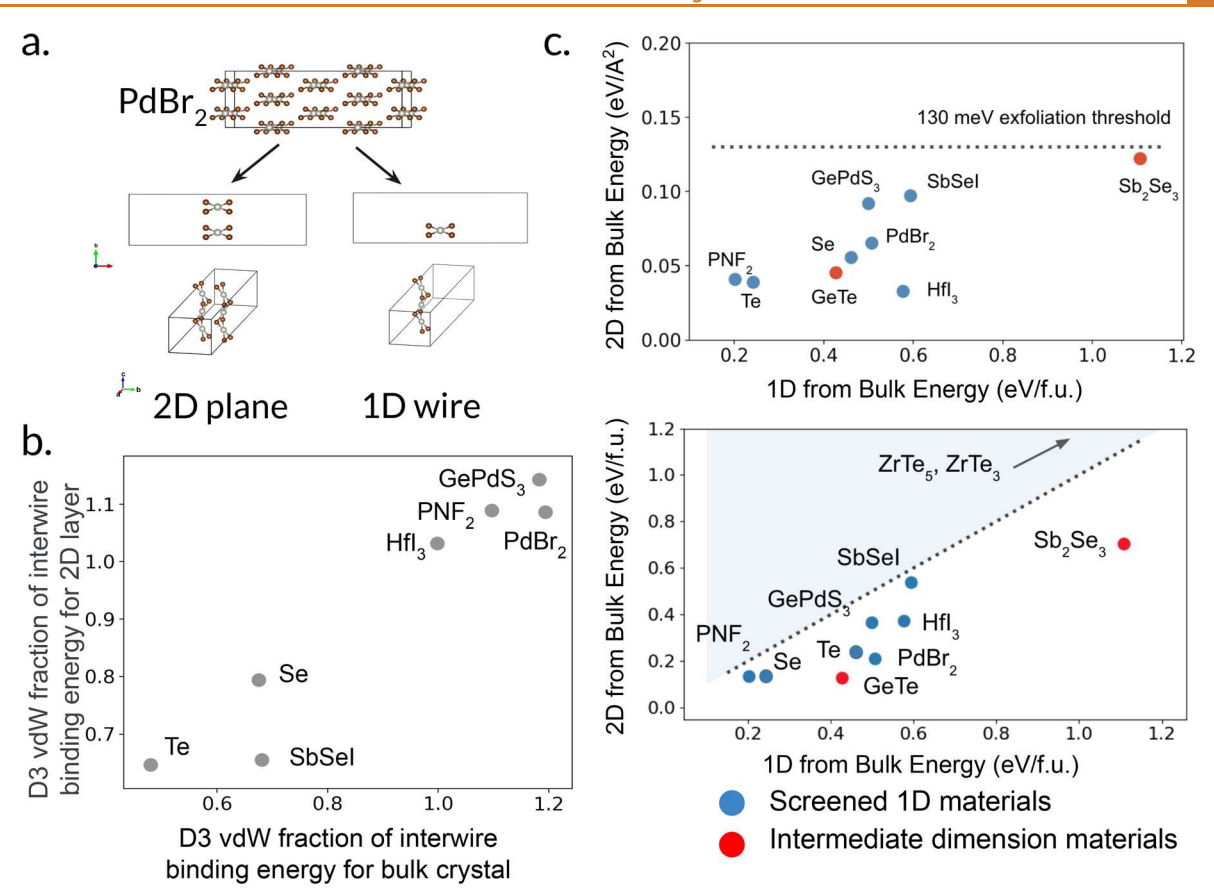


Figure 2. (a) Decomposition of sample geometry $PdBr_2$ into a 2D plane of 1D wire and individual plane of 1D wires. (b) The van der Waals D3 correction component contribution of the total interwire binding energy (PBE+D3) is compared for individual 1D wires and 2D planes of 1D wires. Higher values indicate vdW bonding is more dominant. Proximity of the data to the line y = x suggests minimal anisotropy in the interwire vdW binding component. (c) The binding energy required for extracting a 2D plane of wires from the bulk can be compared to the binding energy required to extract a 1D wire from the bulk per formula unit (top). The energies to extract 2D layers composed of 1D wires are comparable to the energies of known exfoliable 2D layered materials when compared by surface area. In the bottom figure, the dashed 1:1 line suggests a mixture of 1D wires and 2D wire layers might be obtained during mechanical exfoliation for materials close to the line.

nanotube is close to 4 Å in diameter.³² Silicon nanowires have been reported to be fabricated down to 1.3 nm in diameter.³³ However, the stable phase of bulk materials thinned to such dimensions is unclear and requires detailed investigation,³⁴ whereas we expect 1D van der Waals materials will have a favorable chance of exhibiting the same structure as the weakly bonded wire structure present in the bulk.

These materials are also of theoretical interest. They represent two challenging limits of *ab initio* calculations. van der Waals forces between wires involve many-body physics dispersion interactions³⁵ while bonding within a single wire chain can involve strong electronic correlations and electron—phonon coupling. There is potential for the 1D limit to exhibit Luttinger liquid or Wigner crystal behavior, Peierls distortions, or charge and spin density waves. 2D materials have been shown to support similar density wave and exotic low-temperature behavior.³⁶ Studies on the binding energy of these materials are useful to identify systems in which such effects could be realized in the laboratory.³⁷

RESULTS AND DISCUSSION

We leverage data produced in previous work⁶ to identify weakly bonded 2D and 1D layered materials. While twodimensional materials have been further studied with detailed ab initio computations and databases, ^{37–40} there remains limited work on one-dimensional structures. The selected 1D materials are represented in the Materials Project database ⁴¹ with corresponding Inorganic Crystal Structure Database (ICSD) numbers. ⁴² The bulk, nonexfoliated multiwire structures have been previously experimentally synthesized and structurally characterized. Materials are grouped into common families by structural similarity, and a table is included in the Supporting Information (SI), and figures are shown below. Select materials consist of a mixture of wire-like structures with intercalated atoms or molecules.

We choose representative materials from the families and simple wire prototypes to evaluate using density functional theory calculations. Materials from the common structural families SbSeI, ⁴³ TaTlSe₃, ⁴⁴ and HfI₃ ⁴⁵ were selected in addition to PdBr₂, ⁴⁶ PNF₂, ^{47,48} and GePdS₃, ⁴⁹ which display simple, spatially separated wire compositions. We also perform calculations on materials that exhibit wire-like character but insufficient spacing between wires to satisfy the screening criteria of Cheon *et al.* ⁶ for 1D materials. Wire structures GeTe, ⁵⁰ ZrTe₅, ⁵¹ Sb₂Se₃, Ta₂Pd₃Se₈, and members of the transition metal trichalcogenide family NbSe₃ and ZrTe₃ are examined to provide a cohesive comparison and benchmark. SbSeI, Ta₂Pd₃Se₈, ZrTe₃, NbSe, and Sb₂Se₃ have been realized as low-dimensional wires and bundles, whereas ZrTe₅ and

Table 1. Materials and Their Corresponding Band Gaps (in eV) Are Presented for the Bulk Structure, the 2D Layer of 1D Wires, and the Individual 1D Wire Structure (top)^a

material	MP ID/ICSD	bulk direct	indirect	2D direct	indirect	1D direct	indirect	1D relaxed direct	indirect	
HfI_3	mp-568002/23947	0	0	0	0	0	0	0	0	
$PdBr_2$	mp-27857/27443	0.840	0.541	1.072	0.864	1.450	1.273	1.435	1.265	
			Г-М		Γ -(0,0,0.4)					
SbSeI	mp-22996/31292, 35470	1.388	1.378	1.288	1.279	1.346	-	1.766	1.743	
			$(0.2,0,0)$ - Γ							
$GePdS_3$	mp-541785/408505	1.387	1.181	1.608	1.489	1.755	1.654	1.774	1.660	
					Γ -(0.2,0.3,0)		Γ -(0.2,0.2,0.6)		Γ-(0.2,0.2,0.5)	
PNF_2	mp-560008/9684	5.711	-	5.976	-	6.193	6.192	6.190	6.190	
		Г-Г		Г-Г			Γ-(0.02,0.5,0)		Γ -(0.1,0.4,0)	
materia	MP ID/ICSD	ŀ	oulk HS band gap	HS component 1 band gap (formu		rmula) HS	HS component 2 band gap (formula)			
Te ₇ As ₅ I mp-541032/318		0.25		$0.044 (As_2Te_3)$				0.49 (AsTeI)		
Sb ₆ O ₅ F	mp-753233		3.28		2.92 (Sl	OF)		5.25 (SbF	5.25 (SbF ₃)	
InGaTe	e2 mp-20408		0		0 (GaTe ₂)			0 (In)		
TaTlSe	3 mp-12027 0.22		0 (TaSe ₃)				0 (Tl)			

"The values for the relaxed 1D structure are included, where the ion positions are relaxed using DFT upon extraction from the bulk. The smallest direct band gap and indirect band gaps are reported, and the location of the transition is presented for the smallest gap when it is close to a high-symmetry k-point path in reciprocal space. With the exception of HfI_3 and PNF_2 , the materials exhibit sufficiently large changes in band gap between bulk and 1D relaxed wire phases that they are likely to be distinguished using photoluminescence measurements. Similar information is shown for the heterostructures and intercalated structures (bottom). The data suggest electronic band gaps differ sufficiently between bulk and 1D forms of Te_7As_3I and $Sb_6O_3F_8$ to be differentiable based on PL measurements. InGa Te_2 and HfI_3 are both conductors from bulk to 1D forms, suggesting quantum confinement does not open a gap even at nearly atomic widths.

GeTe have only been studied in bulk forms. Images of these materials are indicated in Figures 1 and 4. While members in the same family have similar structures, we note as in the case of the transition metal trichalcogenides, they have been reported to exhibit vastly different electronic properties as verified experimentally. 52,53

Binding Energies. Density functional theory calculations are performed for the bulk structure consisting of multiple wires in the bulk unit cell, 2D plane(s) of 1D wires, and an individual 1D structure shown in Figure 2a. The degree of van der Waals interaction and the lack of strong covalent or electrostatic interactions between adjacent wire structures can be quantitatively estimated by the fraction of the interwire van der Waals correction to the total energy shown in Figure 2b. The vertical and horizontal axes are computed according to $(E_{\text{bulk,vdW}}/f.u._{\text{bulk}} - E_{2D,\text{vdW}}/f.u._{2D})/(E_{\text{bulk,total}}/f.u._{\text{bulk}} - E_{2D,\text{total}}/f.u._{\text{bulk}} - E_{1D,\text{total}}/f.u._{\text{bulk}})$ where E_{vdW} refers to the van der Waals contribution to total energy. We note that an isolated 2D material can interact with itself through vdW type interactions to some extent.

In this analysis, the Perdew–Burke–Ernzerhof (PBE)⁵⁴ functional is assumed to contribute minimally to the van der Waals interactions, as is commonly observed for this functional. Figure 2b indicates that most materials studied here exhibit interwire interactions that are largely if not entirely vdW-based (in the upper right corner), while Te, Se, and SbSeI exhibit a mix of van der Waals and covalent interwire binding. We find that the choice of existing van der Waals corrections between Grimme DFT-D2, Grimme DFT-D3, and Grimme DFT-D3 with Becke–Johnson damping have no significant effect in this trend. ^{55,56} However, some numerical differences are seen when using the vdW-DF2 of Langreth and Lundqvist or the optB88-vdW correction as shown in the SI Table 2 for selected materials. The binding energy calculated with the local density approximation (LDA, ⁵⁹ which is sometimes used as a traditional alternative to PBE

vdW-corrected energies) is provided in SI Table 3b and shown to follow similar trends between wire materials ranking from lowest to highest exfoliation energy. We note the LDA descriptions of vdW are oftentimes qualitatively accurate but expected to be largely serendipitous as compared to the vdW corrections on top of PBE calculations

Figure 2c shows plots of the binding energy, which are expected to be a proxy for the exfoliation energy required to extract a low-dimensional material from the bulk. It is defined to be positive when the bulk structure is more stable. The 1D energy per formula unit is defined as

$$[E_{\text{bulk}} - (N_{\text{bulk}}/N_{\text{1D}})*E_{\text{1D}}]/\text{f.u.}_{\text{bulk}}$$
(1)

where $E_{\rm bulk}$ is the total energy of the bulk structure, and $E_{\rm 1D}$ is the total energy of the 1D structure. $N_{\rm bulk}$ and $N_{\rm 1D}$ are the number of wires units in the bulk and isolated structures respectively, and f.u._{bulk} is the number of formula units present in the bulk structure.

The 2D energy per formula unit is defined analogously with $E_{\rm 2D}$ and $N_{\rm 2D}$. The 2D energy per area is defined with the denominator as the area of the calculation cell in the plane of the 2D layer, instead of f.u._{bulk}. The 2D cleavage plane, if multiple options exist, is taken as the plane with maximal spacing between the layers, which likely also corresponds to the plane with the minimal exfoliation energy for the calculated samples.

The top of Figure 2c indicates that the energy per unit area to remove or exfoliate a 2D layer of 1D wires from the bulk is lower than 130 meV/ $\rm \mathring{A}^2$, which has been used as an approximate exfoliation threshold for 2D materials. ³⁷

The bottom panel of Figure 2c compares the energy per formula unit to extract a 2D layer *versus* a 1D wire from the bulk. This plot shows that the energy required to extract a 1D wire from the bulk is greater than the energy of extracting a 2D plane of 1D wires from the bulk for all materials studied here. However, materials close to the y = x dashed line exhibit extraction energies of the 1D and 2D forms that are

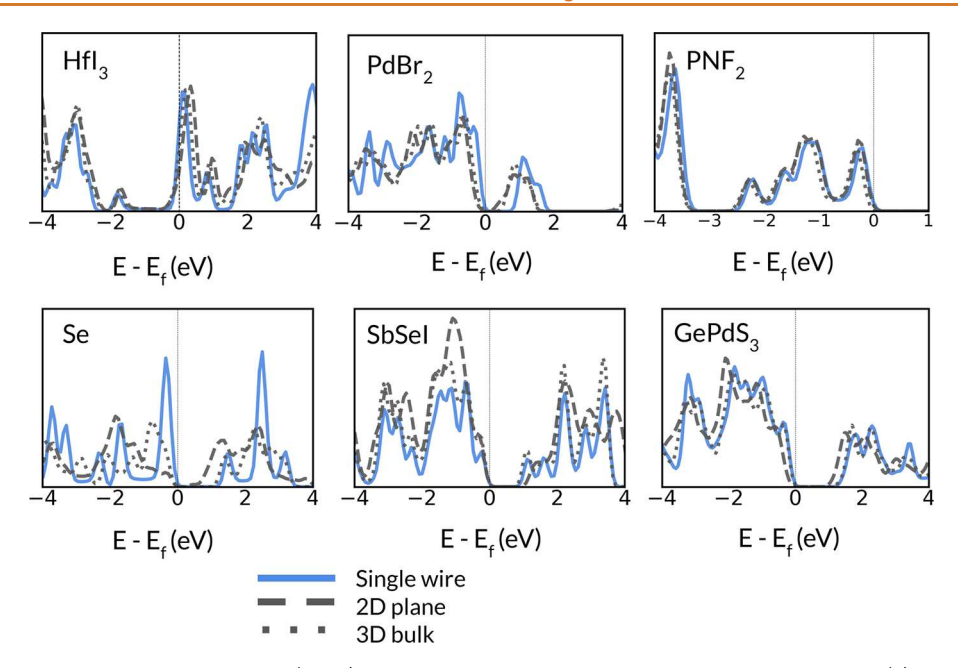


Figure 3. Computed electronic density of states (DOS) comparisons for the wire materials from screening. (a) HfI₃ is calculated to be conducting for the bulk, a 2D plane of wires, and 1D geometries. PdBr₂ displays an increasing band gap with reduced dimensionality, as might be naively expected from quantum confinement. SbSeI shows slight band gap differences between dimensionality, with the band gap largest for bulk, then 1D, then 2D. Se shows the largest change in DOS distribution, while PNF₂ and GePdS₃ largely retain their DOS characteristics from bulk to 1D.

comparable. Therefore, one might expect that mechanical attempts at exfoliation (*e.g.*, rubbing bulk crystals on a surface) could yield a mix of 1D wires and 2D layers for those materials closes to the y = x line.

Perhaps the best candidate for exfoliation of individual 1D chains identified in Figure 2c is PNF₂, which has a low exfoliation energy per unit area for 2D layers (top of Figure 2C) and an exfoliation energy per formula unit of 1D wires that is only slightly more than the 2D sheets (bottom of Figure 2c). Mechanical exfoliation involves rubbing the bulk crystal against a substrate, onto which subcomponents of the bulk will be deposited. In such an experiment, exfoliated 1D wires are expected to be mechanically stabilized by the substrate independent of bending stiffness. Such mechanical stabilization by a substrate is common in thin films.

Electronic Properties. Computed band gaps for bulk, 2D, and 1D forms of of selected materials are presented in Table 1. Similar to how 2D materials span a wide range of electronic characteristics, 1D wires do as well. We find a general trend of increasing band gap as dimensionality is reduced for nonmetallic materials, likely due to quantum confinement.

The electronic band structure of the materials is computed both along the high-symmetry k-point path for bulk materials and momentum-space equivalent of the real-space wire axis for the 1D wires. The electronic band structure decomposed by orbital type and density of states distribution is included in the SI. We find the contribution of the orbitals to the band structure largely stays consistent from the bulk to the single wire, as shown in orbital-decomposed band structures shown in SI Figure 1.

Band calculations for the bulk material indicate that the band gap, if present, is often located close to the path in reciprocal space corresponding to the real-space direction of the wire, which may help explain the relatively small changes of several tenths of an eV in band gap difference between the bulk and an individual 1D wire for most of the materials in Table 1.

The electronic band gap differences between bulk, 2D, and 1D forms of these materials are sufficiently large to enable distinction by photoluminescence (PL). For example, during mechanical exfoliation onto a substrate, PL has potential to enable identification of individual 1D wires and distinguish them from other bulk and layered forms likely to be present on the substrate. Identification of individual exfoliated 1D wires using an optical microscope is possible with 2D layers, but a discernible optical signature is difficult for 1D wires. Table 1 shows that PdBr₂, SbSeI, and GePdS₃ in particular exhibit the largest changes in indirect and direct electronic band gaps between 3D, 2D, and 1D forms, suggesting these might be the easiest to differentiate with PL.

Table 1 further suggests there could be a slight indirect to direct transition upon exfoliation of SbSeI wires from the bulk if the 1D wire structure is unrelaxed, as it may be if constrained by friction on a substrate. However, we find relaxation of the 1D wire structure recovers an indirect gap, suggesting that such a transition may not be observable. The accuracy of these calculations may be insufficient to resolve these differences, neglecting substrate screening, electron—hole, and electron—phonon interaction effects. The SI elaborates on the possibility of this transition.

Figure 3 shows the density of electronic Kohn–Sham states comparison between the bulk, 2D, and 1D components. Some of these materials exhibit a 1D electronic DOS nearly identical to the bulk, in particular Hfl₃ and PNF₂, suggesting minimal electronic interaction between wires in these materials and minimal changes in electronic structure as the materials dimensions are shrunk to nearly atomic scale. The latter is a useful property for some materials applications, like electronic interconnect materials where one would like conductors that maintain their conductivity as film thickness decreases. Hfl₃ in particular is predicted to be a metal in both bulk and 1D forms at this level of theory.

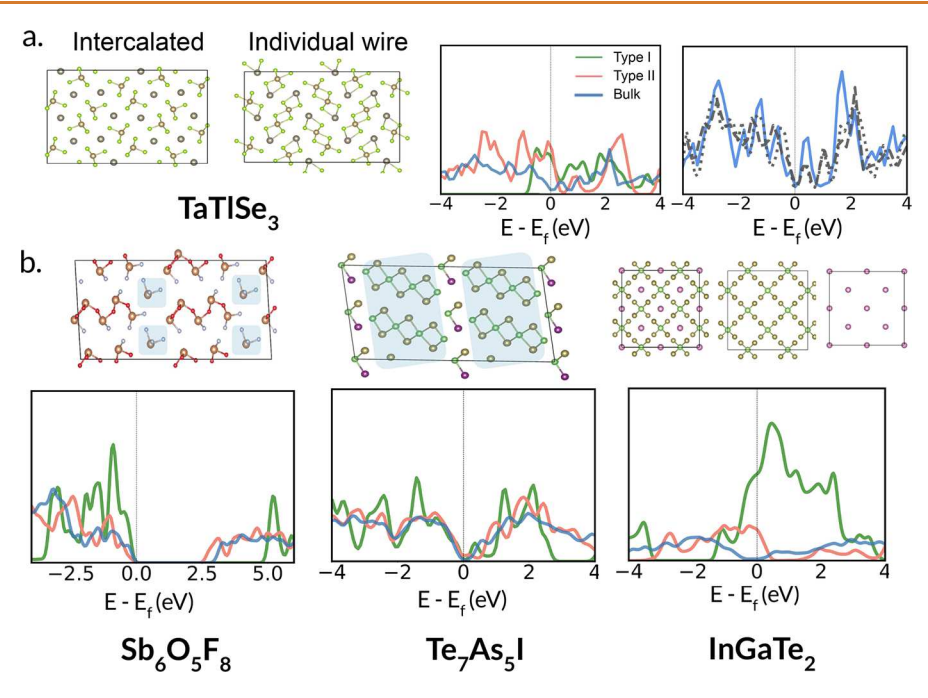


Figure 4. (a) Compound $TaTlSe_3$ can be treated either as an intercalated compound or a wire structure depending on bonding distance thresholds. Electronic density of states plots are shown for both decomposition types. (b) Heterostructure materials $Sb_6O_5F_8$, Te_7Al_5I , and intercalated compound $InGaTe_2$ show different band gaps between the two subcomponent types. The density of states is plotted relative to the Fermi energy level of each individual cluster and bulk structure calculation and is normalized by the number of bands in each calculation.

Heterostructures and Intercalated Ion Wire Structures. In addition to normal wire structures containing chemically and structurally identical chains, there also exist 1D heterostructures in which the bulk structure is composed of wires of differing compositions. These heterostructures are of interest as their bulk forms exhibit intrinsic stacking of two or more subcomponents occurring naturally through synthesis. Bulk heterostructures have been reported as layered materials, where it was found two separate layer-type bands can sum to determine approximate joint bulk structure bands due to relatively weak interlayer interactions. 60

Data mining further reveals intercalated 1D structures, which are distinguished from the two-component heterostructures by one of the components consisting of a single atom (ion) type.

We perform density functional calculations for two sample wire heterostructures Te_7As_5I and $Sb_6O_5F_8$, where the two clustered compositions (Te_2As_3 , TeAsI for Te_7As_5I and SbOF, SbF_3 for $Sb_6O_5F_8$) are evaluated separately. We also consider InGa Te_2 , which appears as 1D wire structures of Ge and Ta with In atoms intercalated. These structures are depicted in Figure 4. Band gaps are summarized in the bottom of Table 1, indicating that the individual subcomponents can exhibit sufficiently different band gaps from the bulk to be distinguishable if a PL signal can be observed.

Many applications for ion intercalation exist, including Li ion battery electrodes, electronic memories, and potentially components of neuromorphic computing systems. These applications have been dominated by layered vdW materials, with considerably less attention paid to inorganic 1D vdW materials of the types studied here. 1D materials may prove to be good candidates for ion intercalation without major structural changes due to their vdW bonded nature.

Relaxation and Stability. The stability of exfoliated wire structures can be described by both thermodynamic stability and mechanical stability. The reported experimental synthesis and characterization of all of the materials studied suggests that they are sufficiently thermodynamically stable for such analysis. To determine the mechanical stability of the materials, we perform individual wire relaxations, phonon calculations, and density functional theory molecular dynamics (DFT-MD) simulations to test for the presence of unstable phonon modes. Individual wire relaxations both with and without the van der Waals correction show slight deviations in bond distances depending on the particular wire type, but we find that the wire structure remained intact for all materials.

Phonon calculations were performed using finite differences with van der Waals corrections and density functional perturbation theory without van der Waals corrections. While certain materials show slight imaginary frequencies, those imaginary frequencies were often present in the bulk compound, known to have been previously synthesized, and often occur at the high-symmetry Γ point.

More tellingly, DFT-MD simulations were performed for the wire structures $\mathrm{Hfl_3}$ and $\mathrm{PdBr_2}$ with three unit cells in the wire direction. These calculations show the wire structures remain bonded, though atoms can exhibit slight distortions and symmetry breaking. The output of the DFT-MD was relaxed again using DFT, and the structure from the DFT-MD simulation remained unchanged from the slightly distorted DFT-MD output structure.

CONCLUSIONS

We find a large number of bulk materials that consist of 1D van der Waals subcomponents have the potential for exfoliation into 1D wires of sub-nm diameters, since their interwire binding energies are comparable to those of 2D van der Waals structures. While there can be changes in the electronic character of the material upon exfoliation, these differences are usually slight compared to breaking apart subcomponents of

bulk compounds. We find that, in many cases, the 1D forms are distinguishable from 2D and bulk forms by photoluminescence techniques, addressing perhaps the biggest challenge of identifying working with such materials upon mechanical exfoliation onto a substrate. These materials have the potential to serve as 1D interconnect replacements and ion intercalation materials for energy storage applications.

METHODS

Geometry optimization and electronic properties calculations are computed using density functional theory (DFT) methods within the generalized gradient approximation (GGA) and PBE exchange correlation functional 54 as performed in the Vienna Ab initio Simulation Package (VASP). 62 The projected augmented wave method 63,64 is used for ion–electron interactions, and the energy cutoff for the plane wave basis is set to 520 eV. All the structures are allowed to relax during this process with a conjugate gradient algorithm until the energy on the atoms is less than 1.0×10^{-4} eV. The DFT-D3 approach proposed by Grimme 55 is used mainly for vdW interactions in the main text. The materials were relaxed for the bulk structure, and the corresponding 1D atomic positions were extracted from this relaxation. A separate relaxation of the 1D wire was also undertaken, and the electronic structure of the resulting wire computed to obtain the second set of band gaps is in Table 1. The calculated band structures are spin-polarized. The LDA functional calculations 59 also use the implementation within VASP.

DFT-MD simulations were carried out for 1 ps with a 2 fs time step and a microcanonical ensemble at 300 K using a 2×2 supercell in the direction perpendicular to the wire and three copies of the primitive unit cell in the wire direction.

ASSOCIATED CONTENT

Supporting Information

The Supporting Information is available free of charge at https://pubs.acs.org/doi/10.1021/acsnano.1c00781.

Table of wires grouped by common families; exfoliation energy calculation details; element-decomposed band structures; van der Waals contribution to interwire binding energy; SbSeI cluster calculations; wire geometries; and DFT-MD relaxation (PDF)

AUTHOR INFORMATION

Corresponding Author

Evan J. Reed — Department of Materials Science and Engineering, Stanford University, Stanford, California 94305, United States; Email: evanreed@stanford.edu

Authors

Yanbing Zhu — Department of Applied Physics, Stanford University, Stanford, California 94305, United States; orcid.org/0000-0002-6850-2926

Daniel A. Rehn — Computational Physics Division, Los Alamos National Laboratory, Los Alamos, New Mexico 87545, United States; © orcid.org/0000-0001-5139-0393

Evan R. Antoniuk — Department of Chemistry, Stanford University, Stanford, California 94305, United States; orcid.org/0000-0002-4273-1974

Gowoon Cheon — Department of Applied Physics, Stanford University, Stanford, California 94305, United States;
o orcid.org/0000-0002-3026-6796

Rodrigo Freitas – Department of Materials Science and Engineering, Massachusetts Institute of Technology, Cambridge, Massachusetts 02139, United States Aditi Krishnapriyan — Computational Research Division, Lawrence Berkeley National Laboratory, Berkeley, California 94720. United States

Complete contact information is available at: https://pubs.acs.org/10.1021/acsnano.1c00781

Notes

The authors declare no competing financial interest.

ACKNOWLEDGMENTS

This work was supported by NSF Grants DMREF-1174625 and DMR-1455050.

REFERENCES

- (1) Geremew, A.; Bloodgood, M. A.; Aytan, E.; Woo, B. W. K.; Corber, S. R.; Liu, G.; Bozhilov, K.; Salguero, T. T.; Rumyantsev, S.; Rao, M. P.; Balandin, A. A. Current Carrying Capacity of Quasi-1D ZrTe3 van der Waals Nanoribbons. *IEEE Electron Device Lett.* **2018**, 39, 735–738.
- (2) Liu, G.; Rumyantsev, S.; Bloodgood, M. A.; Salguero, T. T.; Shur, M.; Balandin, A. A. Low-Frequency Electronic Noise in Quasi-1D TaSe3 van der Waals Nanowires. *Nano Lett.* **2017**, *17*, 377–383.
- (3) Lee, C.-H.; Lee, G.-H.; van der Zande, A. M.; Chen, W.; Li, Y.; Han, M.; Cui, X.; Arefe, G.; Nuckolls, C.; Heinz, T. F.; Guo, J.; Hone, J.; Kim, P. Atomically Thin P-N Junctions with van der Waals Heterointerfaces. *Nat. Nanotechnol.* **2014**, *9*, 676.
- (4) Wang, Q.; Wen, Y.; Cai, K.; Cheng, R.; Yin, L.; Zhang, Y.; Li, J.; Wang, Z.; Wang, F.; Wang, F.; Shifa, T. A.; Jiang, C.; Yang, H.; He, J. Nonvolatile Infrared Memory in MoS2/PbS van der Waals Heterostructures. *Science Advances* 2018, 4, eaap7916.
- (5) Liu, C.; Yan, X.; Song, X.; Ding, S.; Zhang, D. W.; Zhou, P. A Semi-Floating Gate Memory Based on van der Waals Heterostructures for Quasi-Non-Volatile Applications. *Nat. Nanotechnol.* **2018**, *13*, 404.
- (6) Cheon, G.; Duerloo, K.-A. N.; Sendek, A. D.; Porter, C.; Chen, Y.; Reed, E. J. Data Mining for New Two-and One-Dimensional Weakly Bonded Solids and Lattice-Commensurate Heterostructures. *Nano Lett.* **2017**, *17*, 1915–1923.
- (7) Empante, T. A.; Martinez, A.; Wurch, M.; Zhu, Y.; Geremew, A. K.; Yamaguchi, K.; Isarraraz, M.; Rumyantsev, S.; Reed, E. J.; Balandin, A. A.; Bartels, L. Low Resistivity and High Breakdown Current Density of 10 nm Diameter van der Waals TaSe3 Nanowires by Chemical Vapor Deposition. *Nano Lett.* **2019**, *19*, 4355–4361.
- (8) Steinhögl, W.; Schindler, G.; Steinlesberger, G.; Traving, M.; Engelhardt, M. Comprehensive Study of the Resistivity of Copper Wires with Lateral Dimensions of 100 nm and Smaller. *J. Appl. Phys.* **2005**, *97*, 023706.
- (9) Josell, D.; Brongersma, S. H.; Tökei, Z. Size-Dependent Resistivity in Nanoscale Interconnects. *Annu. Rev. Mater. Res.* **2009**, 39, 231–254.
- (10) Rossnagel, S. M.; Kuan, T. S. Alteration of Cu Conductivity in the Size Effect Regime. *J. Vac. Sci. Technol., B: Microelectron. Process. Phenom.* **2004**, 22, 240–247.
- (11) Huang, Q.; Lilley, C. M.; Bode, M.; Divan, R. Surface and Size Effects on the Electrical Properties of Cu Nanowires. *J. Appl. Phys.* **2008**, *104*, 023709.
- (12) Liu, K.; Chien, C. L.; Searson, P. C. Finite-Size Effects in Bismuth Nanowires. *Phys. Rev. B: Condens. Matter Mater. Phys.* 1998, 58, R14681.
- (13) Karim, S.; Ensinger, W.; Cornelius, T. W.; Neumann, R. Investigation of Size Effects in the Electrical Resistivity of Single Electrochemically Fabricated Gold Nanowires. *Phys. E* **2008**, *40*, 3173–3178.
- (14) Dresselhaus, M. S.; Dresselhaus, G.; Eklund, P. C.; Rao, A. M. Carbon Nanotubes. *Phys. Chem. Mater. Low-Dimens. Struct.* **2000**, 23, 331–379.

- (15) Deshpande, V. V.; Bockrath, M. The One-Dimensional Wigner Crystal in Carbon Nanotubes. *Nat. Phys.* **2008**, *4*, 314.
- (16) Nygard, J.; Cobden, D. H.; Lindelof, P. E. Kondo Physics in Carbon Nanotubes. *Nature* **2000**, *408*, 342.
- (17) Bockrath, M.; Cobden, D. H.; Lu, J.; Rinzler, A. G.; Smalley, R. E.; Balents, L.; McEuen, P. L. Luttinger-Liquid Behaviour in Carbon Nanotubes. *Nature* **1999**, *397*, 598.
- (18) Bak, P.; Emery, V. J. Theory of the Structural Phase Transformations in Tetrathiafulvalene-Tetracyanoquinodimethane (TTF-TCNQ). *Phys. Rev. Lett.* **1976**, *36*, 978.
- (19) Krogmann, K. Planar Complexes Containing Metal-Metal Bonds. Angew. Chem., Int. Ed. Engl. 1969, 8, 35-42.
- (20) Su, W.-P; Schrieffer, J. R.; Heeger, A. J. Soliton Excitations in Polyacetylene. *Phys. Rev. B: Condens. Matter Mater. Phys.* 1980, 22, 2099
- (21) Stolyarov, M. A.; Liu, G.; Bloodgood, M. A.; Aytan, E.; Jiang, C.; Samnakay, R.; Salguero, T. T.; Nika, D. L.; Rumyantsev, S. L.; Shur, M. S.; Bozhilov, K. N.; Balandin, A. A. Breakdown Current Density in h-BN-Capped Quasi-1D TaSe3Metallic Nanowires: Prospects of Interconnect Applications. *Nanoscale* **2016**, *8*, 15774—15782.
- (22) Rai, D. P.; Chettri, S.; Shankar, A.; Patra, P. K.; Thapa, R. K. A Comparative Study of 1D Monatomic Fe-Chain and 3D Fe-Bulk within the Density Functional Theory (DFT). *Nanosci. Nanoeng.* **2016**, *4*, 52–57.
- (23) Sun, S.-J.; Yang, P.-Y.; Ju, S.-P.; Lai, Z.-M. Electronic and Structural Properties of Ultrathin Germanium Nanowires by Density Functional Theory Calculations. *J. Appl. Phys.* **2016**, *120*, 195701.
- (24) Torres, J. A.; Tosatti, E.; Dal Corso, A.; Ercolessi, F.; Kohanoff, J. J.; Di Tolla, F. D.; Soler, J. M. The Puzzling Stability of Monatomic Gold Wires. *Surf. Sci.* **1999**, 426, L441–L446.
- (25) Churchill, H. O. H.; Salamo, G. J.; Yu, S.-Q.; Hironaka, T.; Hu, X.; Stacy, J.; Shih, I. Toward Single Atom Chains with Exfoliated Tellurium. *Nanoscale Res. Lett.* **2017**, *12*, 488.
- (26) Pan, H.; Feng, Y. P. Semiconductor Nanowires and Nanotubes: Effects of Size and Surface-to-Volume Ratio. ACS Nano 2008, 2, 2410–2414.
- (27) Peng, B.; Xu, K.; Zhang, H.; Ning, Z.; Shao, H.; Ni, G.; Li, J.; Zhu, Y.; Zhu, H.; Soukoulis, C. M. 1D SbSeI, SbSI, and SbSBr with High Stability and Novel Properties for Microelectronic, Optoelectronic, and Thermoelectric Applications. *Advanced Theory and Simulations* **2018**, *1*, 1700005.
- (28) Zhang, Q.; Liu, C.; Liu, X.; Liu, J.; Cui, Z.; Zhang, Y.; Yang, L.; Zhao, Y.; Xu, T. T.; Chen, Y.; Wei, J.; Mao, Z.; Li, D. Thermal Transport in Quasi-1D van der Waals Crystal Ta2Pd3Se8 Nanowires: Size and Length Dependence. ACS Nano 2018, 12, 2634–2642.
- (29) Lipatov, A.; Loes, M. J.; Lu, H.; Dai, J.; Patoka, P.; Vorobeva, N. S.; Muratov, D. S.; Ulrich, G.; Kastner, B.; Hoehl, A.; Ulm, G.; Zeng, X. C.; Ruhl, E.; Gruverman, A.; Dowben, P. A.; Sinitskii, A. Quasi-1D TiS3 Nanoribbons: Mechanical Exfoliation and Thickness-Dependent Raman Spectroscopy. ACS Nano 2018, 12, 12713–12720.
- (30) Song, H.; Li, T.; Zhang, J.; Zhou, Y.; Luo, J.; Chen, C.; Yang, B.; Ge, C.; Wu, Y.; Tang, J. Highly Anisotropic Sb2Se3 Nanosheets: Gentle Exfoliation from the Bulk Precursors Possessing 1D Crystal Structure. *Adv. Mater.* **2017**, *29*, 1700441.
- (31) Zhao, X.; Liu, Y.; Inoue, S.; Suzuki, T.; Jones, R. O.; Ando, Y. Smallest Carbon Nanotube Is 3 Å in Diameter. *Phys. Rev. Lett.* **2004**, 92, 125502.
- (32) Hayashi, T.; Kim, Y. A.; Matoba, T.; Esaka, M.; Nishimura, K.; Tsukada, T.; Endo, M.; Dresselhaus, M. S. Smallest Freestanding Single-Walled Carbon Nanotube. *Nano Lett.* **2003**, *3*, 887–889.
- (33) Ma, D. D. D.; Lee, C. S.; Au, F. C. K.; Tong, S. Y.; Lee, S. T. Small-Diameter Silicon Nanowire Surfaces. *Science* **2003**, 299, 1874–1877.
- (34) Ponomareva, I.; Menon, M.; Srivastava, D.; Andriotis, A. N. Structure, Stability, and Quantum Conductivity of Small Diameter Silicon Nanowires. *Phys. Rev. Lett.* **2005**, *95*, 265502.
- (35) Tkatchenko, A. Current Understanding of van der Waals Effects in Realistic Materials. Adv. Funct. Mater. 2015, 25, 2054–2061.

- (36) Wilson, Jl A; Di Salvo, F. J.; Mahajan, S. Charge-Density Waves and Superlattices in the Metallic Layered Transition Metal Dichalcogenides. *Adv. Phys.* **1975**, *24*, 117–201.
- (37) Mounet, N.; Gibertini, M.; Schwaller, P.; Campi, D.; Merkys, A.; Marrazzo, A.; Sohier, T.; Castelli, I. E.; Cepellotti, A.; Pizzi, G.; Marzari, N. Two-Dimensional Materials from High-Throughput Computational Exfoliation of Experimentally Known Compounds. *Nat. Nanotechnol.* **2018**, *13*, 246.
- (38) Haastrup, S.; Strange, M.; Pandey, M.; Deilmann, T.; Schmidt, P. S; Hinsche, N. F; Gjerding, M. N; Torelli, D.; Larsen, P. M; Riis-Jensen, A. C; Gath, J.; Jacobsen, K. W; Jørgen Mortensen, J.; Olsen, T.; Thygesen, K. S The Computational 2D Materials Database: High-Throughput Modeling and Discovery of Atomically Thin Crystals. 2D Mater. 2018, 5, 042002.
- (39) Choudhary, K.; Kalish, I.; Beams, R.; Tavazza, F. High-Throughput Identification and Characterization of Two-Dimensional Materials Using Density Functional Theory. *Sci. Rep.* **2017**, *7*, 5179.
- (40) Ashton, M.; Paul, J.; Sinnott, S. B.; Hennig, R. G. Topology-Scaling Identification of Layered Solids and Stable Exfoliated 2D Materials. *Phys. Rev. Lett.* **2017**, *118*, 106101.
- (41) Jain, A.; Ong, S. P.; Hautier, G.; Chen, W.; Richards, W. D.; Dacek, S.; Cholia, S.; Gunter, D.; Skinner, D.; Ceder, G.; Persson, K. A. Commentary: The Materials Project: A Materials Genome Approach to Accelerating Materials Innovation. *APL Mater.* **2013**, *1*, 011002.
- (42) Bergerhoff, G.; Hundt, R.; Sievers, R.; Brown, I. D. The Inorganic Crystal Structure Database. *J. Chem. Inf. Comput. Sci.* **1983**, 23, 66–69.
- (43) Voutsas, G. P.; Rentzeperis, P. J. The Crystal Structure of Antimony Selenoiodide, SbSeI. *Zeitschrift Für Kristallographie-Crystalline Materials* **1982**, *161*, 111–118.
- (44) Teske, C. L.; Bensch, W.; Benea, D.; Minar, J.; Perlov, A.; Ebert, H. Preparation, Crystal Structure, Properties, and Electronic Band Structure of TlTaSe3. *Z. Naturforsch.*, B: J. Chem. Sci. 2005, 60, 858–866.
- (45) Dahl, L. F.; Chiang, T.-I; Seabaugh, P. W.; Larsen, E. M. Structural Studies of Zirconium Trihalides and Hafnium Triiodide. *Inorg. Chem.* **1964**, *3*, 1236–1242.
- (46) Brodersen, K.; Thiele, G.; Gaedcke, H. Die Konstitution Des Palladium (II)-Bromids. Z. Anorg. Allg. Chem. 1966, 348, 162–167.
- (47) Allcock, H. R.; Kugel, R. L.; Stroh, E. G. Phosphonitrilic Compounds. XIII. Structure and Properties of Poly (Difluorophosphazene). *Inorg. Chem.* **1972**, *11*, 1120–1123.
- (48) Elias, A. J.; Twamley, B.; Haist, R.; Oberhammer, H.; Henkel, G.; Krebs, B.; Lork, E.; Mews, R.; Shreeve, J.'n. M. Tetrameric Fluorophosphazene, (NPF2)4, Planar or Puckered? *J. Am. Chem. Soc.* **2001**, *123*, 10299–10303.
- (49) Johrendt, D.; Tampier, M. PdGeS3—A Novel One-Dimensional Metathiogermanate. *Chem. Eur. J.* **1998**, *4*, 1829—1833.
- (50) Onodera, A.; Sakamoto, I.; Fujii, Y.; Mori, N.; Sugai, S. Structural and Electrical Properties of GeSe and GeTe at High Pressure. *Phys. Rev. B: Condens. Matter Mater. Phys.* **1997**, *56*, 7935.
- (51) Lv, Y.-Y.; Zhang, F.; Zhang, B.-B.; Pang, B.; Yao, S.-H.; Chen, Y.B.; Ye, L.; Zhou, J.; Zhang, S.-T.; Chen, Y.-F. Microstructure, Growth Mechanism and Anisotropic Resistivity of Quasi-One-Dimensional ZrTe5 Crystal. *J. Cryst. Growth* **2017**, *457*, 250–254.
- (52) Srivastava, S. K.; Avasthi, B. N. Preparation, Structure and Properties of Transition Metal Trichalcogenides. *J. Mater. Sci.* **1992**, 27, 3693–3705.
- (53) Island, J. O; Molina-Mendoza, A. J; Barawi, M.; Biele, R.; Flores, E.; Clamagirand, J. M; Ares, J. R; Sanchez, C.; van der Zant, H. S J; D'Agosta, R.; Ferrer, I. J; Castellanos-Gomez, A. Electronics and Optoelectronics of Quasi-1D Layered Transition Metal Trichalcogenides. 2D Mater. 2017, 4, 022003.
- (54) Perdew, J. P.; Burke, K.; Ernzerhof, M. Generalized Gradient Approximation Made Simple. *Phys. Rev. Lett.* **1996**, *77*, 3865.
- (\$\$) Grimme, S.; Antony, J.; Ehrlich, S.; Krieg, H. A Consistent and Accurate ab Initio Parametrization of Density Functional Dispersion

- Correction (DFT-D) for the 94 Elements H-Pu. J. Chem. Phys. 2010, 132, 154104.
- (56) Grimme, S.; Ehrlich, S.; Goerigk, L. Effect of the Damping Function in Dispersion Corrected Density Functional Theory. *J. Comput. Chem.* **2011**, 32, 1456–1465.
- (57) Klimes, J.; Bowler, D. R; Michaelides, A. Chemical Accuracy for the van der Waals Density Functional. *J. Phys.: Condens. Matter* **2010**, 22, 022201.
- (58) Lee, K.; Murray, E. D.; Kong, L.; Lundqvist, B. I.; Langreth, D. C. Higher-Accuracy van der Waals Density Functional. *Phys. Rev. B: Condens. Matter Mater. Phys.* **2010**, 82, 081101.
- (59) Perdew, J. P.; Zunger, A. Self-Interaction Correction to Density-Functional Approximations for Many-Electron Systems. *Phys. Rev. B: Condens. Matter Mater. Phys.* **1981**, 23, 5048.
- (60) Antoniuk, E. R.; Cheon, G.; Krishnapriyan, A.; Rehn, D. A.; Zhou, Y.; Reed, E. J. New Assembly-Free Bulk Layered Inorganic Vertical Heterostructures with Infrared and Optical Bandgaps. *Nano Lett.* **2019**, *19*, 142–149.
- (61) Fuller, E. J.; Keene, S. T.; Melianas, A.; Wang, Z.; Agarwal, S.; Li, Y.; Tuchman, Y.; James, C. D.; Marinella, M. J.; Yang, J. J.; Salleo, A.; Talin, A. A. Parallel Programming of an Ionic Floating-Gate Memory Array for Scalable Neuromorphic Computing. *Science* **2019**, 364, 570–574.
- (62) Kresse, G.; Furthmuller, J. Efficient Iterative Schemes for ab Initio Total-Energy Calculations Using a Plane-Wave Basis Set. *Phys. Rev. B: Condens. Matter Mater. Phys.* **1996**, *54*, 11169.
- (63) Blöchl, P. E. Projector Augmented-Wave Method. *Phys. Rev. B: Condens. Matter Mater. Phys.* **1994**, *50*, 17953.
- (64) Kresse, G.; Joubert, D. From Ultrasoft Pseudopotentials to the Projector Augmented-Wave Method. *Phys. Rev. B: Condens. Matter Mater. Phys.* **1999**, *59*, 1758.